Peltonen, A.; Etula, J.; Seitsonen, J.; Engelhardt, P.; Laurila, T.

Three-Dimensional Fine Structure of Nanometer-Scale Nafion Thin Films

Published in:
ACS Applied Polymer Materials

DOI:
10.1021/acsapm.0c01318

Published: 12/02/2021

Document Version
Publisher's PDF, also known as Version of record

ACS APPLIED POLYMER MATERIALS

ACS EDITORS' CHOICE

pubs.acs.org/acsapm

Article

Three-Dimensional Fine Structure of Nanometer-Scale Nafion Thin Films

A. Peltonen,* J. Etula, J. Seitsonen, P. Engelhardt, and T. Laurila

Cite This: *ACS Appl. Polym. Mater.* 2021, 3, 1078−1086

Read Online

ACCESS | Metrics & More | Article Recommendations | Supporting Information

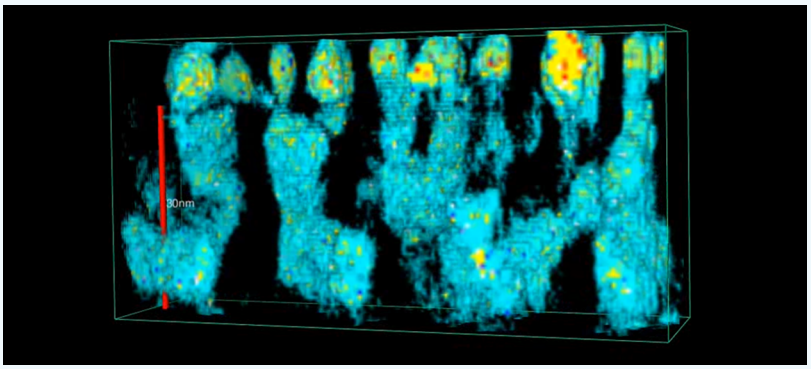

ABSTRACT: Nafion is a widely used polymer membrane in various applications ranging from advanced energy solutions to sensing of biomolecules. Despite the intensive research carried out over the years to reveal and understand the fine structure of Nafion, its structural features, especially as nanometer-scale films, are not unambiguously known. In this paper, we use room temperature scanning transmission electron microscopy (STEM) tomography complemented by glancing incidence small-angle X-ray scattering (GISAXS) and TEM at low temperatures to reveal the fine structure of thin (10−100 nm) unannealed Nafion films. The results from the detailed three-dimensional reconstructions obtained show that (i) the phase fractions of the hydrophobic and hydrophilic parts of the polymer are somewhat thickness-dependent, changing from 0.65/0.35 to about 0.7/0.3 when moving from 100 to 10 nm thick films; (ii) the channel diameters show a range of values from 3 to 6 nm in all the films independent of their thickness; (iii) the average distances between the hydrophilic channels inside the film have distributions centered around 12 nm (in 10 nm films), 15 nm (in 30 nm films), and 7 nm (in 100 nm films); (iv) in the thickest films, the hydrophilic channels exhibit higher interconnectivity and some of the channels appear to end within the Nafion film instead of going through the films; and (v) there are some confinement effects caused by the hydrophilic SiO_2 surface in the case of 10 and 30 nm thick films shown by the tendency of the hydrophilic channels to move horizontally near the substrate. Furthermore, a stable room temperature STEM tomography imaging method for Nafion films and a sample preparation method that preserves the characteristics of the hydrated morphology of Nafion in the dry state are demonstrated. These results provide a deeper understanding of the fine structure of Nafion thin films and provide a better means to characterize and understand their properties in different applications.

KEYWORDS: *Nafion, thin films, STEM, tomography, 3D structure, reconstruction*

INTRODUCTION

The detailed morphology of Nafion (perfluorosulphonic acid polymer) is of great interest to understand its characteristic ionic conducting properties when used as thin-film membranes.[1] The detailed structural knowledge of the film would be an extremely useful tool for predicting the performance and designing new applications based on these materials. The composition of Nafion consists of a hydrophobic semicrystalline Teflon-like backbone with sidechains terminating in hydrophilic sulfonic ($-SO_3H$) groups that give rise to ion-transport properties of the material. The Teflon backbone gives Nafion exceptional mechanical stability, low gas permeability, and great chemical and thermal stability, resulting in a melting point of around 270 °C. When adequately hydrated, Nafion membranes are highly conductive for cations, which are thought to be transported along the hydrophilic and negatively charged channels composed of sulfonic groups. The ionic conduction of Nafion is heavily dependent on the amount of absorbed water,[2−5] nanostructure of the material,

Received: November 27, 2020
Accepted: January 7, 2021
Published: January 28, 2021

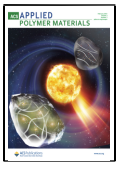

https://dx.doi.org/10.1021/acsapm.0c01318
ACS Appl. Polym. Mater. 2021, 3, 1078−1086

and especially on the connectivity of the ion channels. Because of its ionic properties, Nafion has been used in fuel cells,[1−3,5−12] polymer electrolytes,[5] bio sensors,[13] Donnan dialysis cells,[14] acidic catalyst synthetics,[14,15] modification of electrode surfaces,[3] electrochemical sensors,[1] and drug release.[16]

Although Nafion has been used and studied extensively over the decades, its structure−property relationships, especially when utilized as nanometer-scale thin films, are still not unambiguously known. A variety of study methods have included swelling measurements,[6,17,18] small-angle x-ray scattering (SAXS),[7−12,15,19−22] grazing-incidence small-angle X-ray scattering (GISAXS),[23,24] atomic force microscopy,[25−29] electrostatic force microscopy,[30] impedance spectroscopy, contact angle measurements, transmission electron microscopy (TEM),[31−37] cryo-electron microscopy (cryo-EM), diffraction, energy-dispersive X-ray spectroscopy, neutron scattering,[38−41] neutron reflectometry,[42] infrared spectroscopy,[43,44] and ionic diffusion.[45,46] To summarize the extensive literature on Nafion, these numerous studies have produced a variety of simulation results,[14] reconstructions, and models,[47−52] which often comprise round and/or cylindrical shapes, that have been used to predict the film transport coefficient,[53] proton transport[54,55] and structure. However, there exists no consensus as to which of the several models best describes clustering in Nafion or whether the assumed channels in Nafion are connected and precisely in which way. Thus, there is a clear need for direct observations about the structure of Nafion to resolve at least some of the controversies in the literature.

The difficulty of obtaining direct images of insulating and beam-sensitive materials like Nafion stems from typical imaging methods involving high-energy beams of charged particles, primarily electrons used in electron microscopy. The charging and polymer microstructure deforming beam damage of Nafion in TEM makes high-resolution imaging an excruciating experience, as discussed by Rieberer,[31] Porat,[33] Yakovlev,[37] and Allen.[36] Methods to overcome beam damage by cooling, using lower doses, lower exposure time, under focus, carbon coating layer, and thinner samples, have been used, but little is reported of successful stabilization of sensitive ionomers. Thus far, all the methods involving two-dimensional (2D) imaging have been limited to low magnifications, and results discussed are prone to interpretations. In some TEM studies, it has been possible to see some 3−5 nm circular clusters, and RuO_4-positive staining has revealed a typical two-phase copolymer structure,[32−35] yet these results have not been conclusive. Another problem involving popular TEM methods is the capturing of an image of the material from one direction only and trusting that the representation of the material in that projection and the following interpretations of the underlying structure are valid. The reality in such an arrangement is that TEM images from three-dimensional (3D) objects produce superimposed 2D orthogonal projections. This limits the usability of 2D images and imposes uncertainty for any interpretations of the 3D reality.

Based on the literature information, most of the investigations of Nafion have been carried out using micrometer range films that are far too thick to be used in many biosensing applications. For example, in the case of glutamate detection, which is an important neurotransmitter in the mammalian brain, temporal resolution must be in the range of 10 ms or less.[56] Thus, in these cases, the filtering membrane must be less than 1 μm thick (and if possible, sub-100 nm in thickness), as otherwise it would impose serious mass transfer delays that would drastically compromise the reliable operation of the biosensor.

The most conclusive electron microscopy study of thin-film Nafion structure so far by Allen[36] et al. revealed the random morphology of sub-micrometer hydrated films through cryo-electron tomography and 3D reconstruction. Unfortunately, in Allen's study, only one thickness of the Nafion film (100 nm) was investigated, and no attempts to study very thin (tens of nm) films were done. Moreover, no systematic slicing of the 3D constructions was done, and therefore, the detailed structural information remains elusive. Thus, the main objectives of the present research are to (i) assess the 3D fine structure of the Nafion membranes directly in the sub-100 nm thickness region and consequently to (ii) find out if the morphology of the membranes would drastically change as we approach very thin (10 nm) films by using a STEM technique, and (iii) find a stable room temperature STEM imaging method for Nafion. This information, to the best of our knowledge, is missing in the current literature.

RESULTS AND DISCUSSION

GISAXS profiles were obtained first to relate the electron microscopy and tomography results to common scattering models available in the literature. GISAXS patterns obtained from Nafion films hydrated by water droplets, as shown in Figures S1a and S2−S8, show typical scattering peaks between q = 1.5 and 2.0 nm^{-1} corresponding to Nafion ionomer domains, as commonly reported in the literature.[57,58] Compared to dry films, swelling due to water intake shifts the peaks to lower q-values and increases the intensity, that is, the scattering contrast between sulfonated domains and the fluorinated backbone. Moisture intake due to water droplets introduced to the sides of the beam footprint increased the film thicknesses of the hydrated films by about 10−15% in comparison to the dry ones as measured by in situ X-ray reflectivity (XRR) (Figure S1b and Table S1).

TEM investigations at low temperature were pursued next in order to obtain further understanding of the film morphologies. It is to be noted here that in contrast to the GISAXS results, Nafion structures shown in Figures S9 and S10 are assumed to be dry because the water will be evaporated in the TEM vacuum chamber to a large degree. Clustering was also observed in this dry polymer state. Based on the top-view TEM micrographs (Figures S9 and S10), it is very difficult to evaluate the volume fractions of the hydrophobic and hydrophilic parts, as the visual information from the whole structure is overlaid, strongly biasing the estimation process (see below and the Supplementary Information).

The single tilt TEM images of the intact Nafion film indicated a uniform fine structure compatible with a view where channels are permeating the film. When imaged perpendicular to the plane, most of the channels appeared as spheres, indicating directionality, although some channels were observed along the plane as well. To further characterize the fine structure of the Nafion film, a cross-sectional sample was produced using an ultramicrotome. In the cross-sectioned sample, most channels appeared elongated as could be expected by assuming that the channels have a preferred direction perpendicular to the film surface. Measurement of channels yielded an average approximate channel diameter of 3.2 ± 0.5 nm. While the minimum diameter measured was 2.5

https://dx.doi.org/10.1021/acsapm.0c01318
ACS Appl. Polym. Mater. 2021, 3, 1078−1086

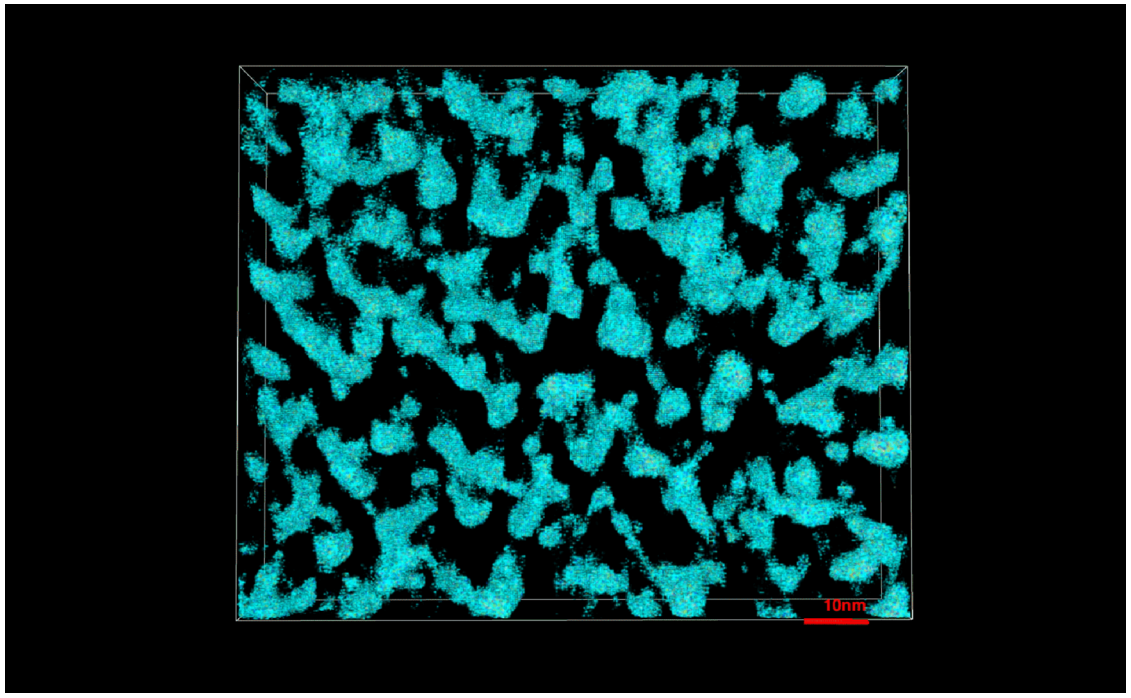

Figure 1. 3D reconstruction top view of the 10 nm thick Nafion thin film. The voxel size of the reconstruction is 0.337 nm and the scale bar is 10 nm. See the associated videos of the tomograms in Zenodo.[63]

nm and maximum 6.0 nm, the number of such observed outliers was very low. It is to be noted that the measurement of the channel dimensions from individual images is at best an approximation due to the random undulation of the channels and the high thickness of the film relative to the diameter of the channels. Additionally, the cross-sectioned film sample may suffer from compression and shearing artifacts introduced by the ultramicrotomy, which could skew the data. Finally, depending on the focusing conditions, the contrast of hydrophilic/hydrophobic parts is different, making any quantitative assessment of the structure practically impossible (see Table S2 for more details).

As the information gained from GISAXS and TEM at low temperature did not give us reliable structural information, STEM tomography investigations were carried out to achieve a view of Nafion morphology in high detail. It is assumed here that the STEM image tilt series were acquired from dry Nafion membranes because of the fact that they were imaged under vacuum in an electron microscope chamber. However, as the negative staining with uranyl formate (UF) $[UO_2(CHO_2)_2 \cdot H_2O]$ was very well absorbed into the channels and was permeated evenly throughout the film independent of film thickness (10−100 nm), one may expect that the hydrated state of the Nafion film is at least partly retained also under the present imaging conditions. As the rodlike uranyl ion $[UO_2^{2+}]$ has such a small size (length ∼500 pm) in comparison to that of the expected size of the hydrophilic channel as well as a high positive charge, it can be expected to form a thin layer with high affinity to sulphonyl-covered walls of the Nafion channels. The fact that reconstructions show complete filling of channels, and not just on the walls, suggests that this simple picture may be somewhat incomplete. In fact, UF has been shown by computer simulations and experiments to form uranyl-formate-uranyl polymeric chains in solutions.[59] This means that more UF than is needed to cover the channel walls will be pulled and bonded into the channels as chains, thus filling them close to the maximum. In dissolved uranyl, five equatorial water ligands bind to a uranyl ion. The question is, then, whether the vacuum in the electron microscope chamber ($1.5\ e^{-5}$ Pa) is sufficient to detach all or some of these water molecules, or do they at least partly remain inside the Nafion channels bonded to uranyl. Furthermore, we cannot completely exclude the influence of capillary forces contributing to filling of channels either. Thus, we anticipate that the Nafion channels contain plenty of uranyl and accompanied formate mixture, with possibly some water molecules still present. The coarse alignment used was enough to reveal negatively stained channels in a manner appropriate for the purpose, and no further alignment was needed. Because of the high UF concentration, the hydrophilic channels showed higher density over the backbone material. In the control samples without UF, the channels were not visible, confirming that UF is the only source of clear contrast in the channels of UF-stained samples. On the other hand, the fiducial Au markers used in STEM imaging showed higher density than UF-saturated channels because of being pure solid gold, thus producing a well-defined contrast. The density histogram of the reconstructions is represented in a standard way by showing decreasing density from red (fiducial markers) to blue (channels). The thin Teflon-like backbone material is filtered invisible by cut off at lowest densities, thus leaving only the stained channels visible. The fact that UF is not swelling or mixing with the bulk, fiducial markers show such nice round shapes and that Nafion exhibits high phase contrast in final reconstructions shows that no observable irradiation damage occurs while the tilt series is collected. In all samples, there was an overall tendency for cationic fiducial markers to seek an available channel in vicinity, and then stay there and block it. Fiducial markers were found forming either larger clusters or single markers that were always found on top of a channel as expected. As discussed, the cationic Au particles are themselves hydrophilic and are carrying water within the ligand layer

https://dx.doi.org/10.1021/acsapm.0c01318
ACS Appl. Polym. Mater. 2021, 3, 1078−1086

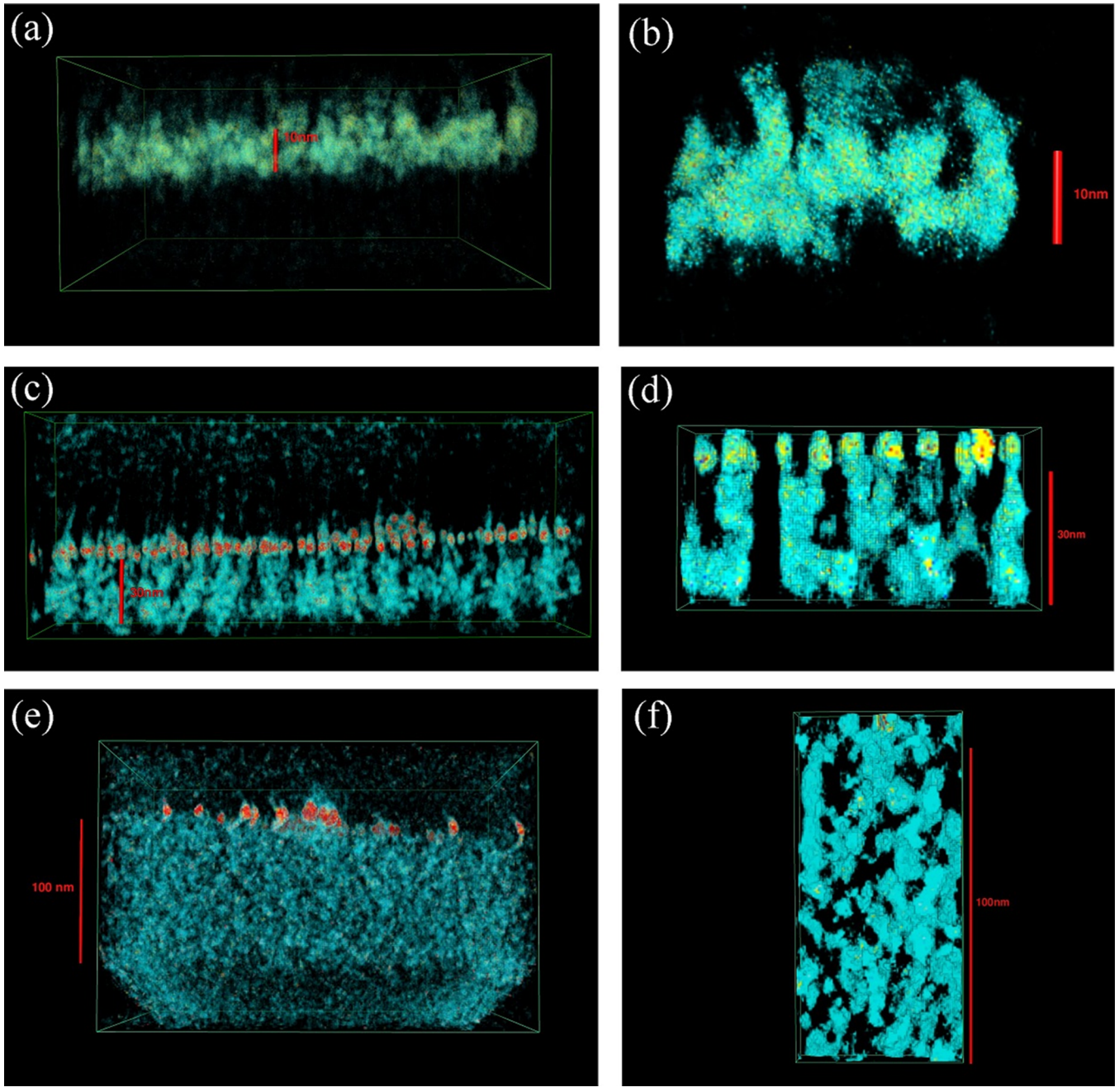

Figure 2. STEM tomography reconstructions showing (a) cross section of a 10 nm thick thin film without Au markers. The scale bar is 10 nm. (b) Side view of a single channel in a 10 nm thin film. The voxel size is 0.337 nm and the scale bar is 10 nm. (c) Cross section of a 30 nm thick thin film. The red dots on the top surface are the 5 nm fiducial gold markers. The voxel size is 0.27 nm, and the scale bar is 30 nm. (d) Closeup of a few single channels in a 30 nm thin film. The yellow dense spherical shapes on the top surface are 5 nm fiducial gold markers. (e) Cross section of a 100 nm thin film. The voxel size is 0.27 nm, and the scale bar is 100 nm. The red spherical objects on the top surface are 5 nm fiducial gold markers. The v-shape patterns at the bottom corners are the edges of the tomogram, which become partly visible at this scale. (f) Interconnected single channels in a 100 nm thick thin film. Gold markers on the top surface are barely visible. See the associated videos of the tomograms in Zenodo.[63]

attached to their surface. Thus, the Au particles were attracted toward the hydrophilic channels by a combined electrostatic and hydrophilic interactions. It is interesting to note that the 5 nm sized Au markers were just barely too large to be absorbed inside the channels.

The STEM tomography results (Figures 1 and 2) for the overall film structures are rather consistent among all the prepared thicknesses (10, 30, and 100 nm) and can all be described as "bulk-like," as reported by Allen.[36] The detailed channel shapes, distances, and distribution are, however, dependent on the film thickness. As revealed by the large number of slices taken through the 3D STEM reconstructions (see the Supplementary Information and images in Zenodo[60] for details), there is a significant variation in the channel diameters throughout the films. Based on averaging over multiple measurements, the hydrophilic channels measure approximately 3−6 nm in diameter in all the films and tend to form an undulating and anisotropic interconnected mesh. The values determined from these direct observations are

https://dx.doi.org/10.1021/acsapm.0c01318
ACS Appl. Polym. Mater. 2021, 3, 1078−1086

Table 1. Structural Information of Nafion Films

hydrated	channel width	hydrophilic phase fraction	mean distance between channels	film thickness	analysis technique	reference
partly owing to strong UF penetration into the channels	3−6 nm	0.3−0.35 (10−100 nm)	distribution centered at 12 nm (10 nm film), 15 nm (30 nm film), and 7 nm (100 nm film)	10, 30 and 100 nm	STEM tomography with UF staining at room temperature	this work
yes	∼6 nm	NA	∼8 nm	175 μm	SAXS and SANS[a]	18
yes	3−5 nm	NA	NA	175 μm	SAXS and SANS[a]	8
yes	∼6 nm	NA	NA	175 μm	SAXS	10
yes	∼5.7 nm	NA	NA	50 nm	SAXS	24
no	∼5 nm	NA	NA	30−40 nm	TEM	33
yes	∼5 nm	0.55	NA	100 nm	cryo-TEM tomography	36
to 20%	∼1.8−3.5	NA	NA	NA	simulations of literature SAXS data	50

[a]Small-angle neutron scattering

consistent with those obtained from the more indirect GISAXS and TEM at low temperature methods (see above).

Figure 2b,d,f shows a more detailed view of the Nafion fine structure. The channel size determined (varying between 3 and 6 nm; see details in the Supplementary Information) corresponds to that reported for wetted Nafion, thus indicating that UF adsorption most likely preserves the swelled morphology of the hydrophilic channels also in the dry state at least to some degree. The fact that fiducial Au markers with about 5 nm diameter could not enter the channels indicates that the upper limit of the channel width distribution might be slightly less than 6 nm, but the evidence is not conclusive. There appears to be no major texture or preferred orientation effects in the films as expected based on the fabrication method. The direct STEM observations from UF-stained thin Nafion films in our study seem to fit best to the cluster network model discussed in a recent review by Kusoglu and Weber.[61]

The top view of the 10 nm Nafion reconstruction (Figure 1) has similar patterns that are seen in our earlier TEM results (see Figures S9 and S10) and RuO_4 vapor-stained films imaged with TEM by Xue.[35] No three-phase interfaces were observed contrary to that proposed by some theoretical three-phase models.[45,62] No visible changes in phase separation for decreasing film thicknesses was observed. The 10 nm membrane revealed excellent contrast and separation between hydrophilic−hydrophobic phases, and Figure 1 shows clear order in the film, in contrast to what was suggested by earlier GISAXS results obtained by Modestino[24] et al. The hydrophilic−hydrophobic copolymer phase ratio as determined from the large number of slices through the 3D STEM reconstruction (see Figures S11−S28, and Table S3 for details) was roughly 0.3/0.7 in the 10 nm thick film, changing gradually to about 0.35/0.65 in the thickest 100 nm film. It is to be noted that just by purely inspecting the overlaid view of the complete reconstruction (Figure S22), it is not possible to reliably evaluate the phase fractions, and a strong bias toward a ratio of about 0.5/0.5 is evident. This is also the case when TEM micrographs from one direction (see, e.g., Figures S9 and S10) are used to assess volume fraction of the phases. Furthermore, as the slices through the complete reconstruction show (Figures S11−S28), the ones taken near the surface area (both top and bottom) give rather different values for the volume phase fractions than the slices further inside the film. This exemplifies the problems of estimating the phase fractions and casts some doubts over the values reported in the literature.[36]

As the film thickness increases to 100 nm, the transparency for electrons decreases, and the noise in the collected tomography data starts to increase (Figure 2e). In the 100 nm film, the random orientation of channels was more evident than in the thinner films and extensive branching connecting channels into a network was observed. One can also notice how some of the channels appeared to end inside the film instead of going through. No change in the channel diameter distribution was detected. There is also no pronounced orientation effects in this thickness range nor influence from the Si/SiO_2 substrate consistent with observations reported by Kushner et al.[64]

The major difference between films of 10 and 100 nm is in the branching of the channels being more extensive in thicker films, and in the 100 nm thick films, more channels appear to terminate inside the film without going through than in the thinner films (10 and 30 nm). Furthermore, when the film thickness decreases down to 10−30 nm, some confinement effects emerge. Most notably, near the substrate/film interface, hydrophilic channels start to orient horizontally, which is not seen in 100 nm thick films. The confinement effects in 10 to 30 nm thick films observed here directly are consistent with the computational results reported by Vanya et al.[65] and Sengupta et al.[66] and more indirect experimental results from below 60 nm thick films by Eastman et al.[67] and Kim et al.[68] However, we did not observe the formation of a distinct truncated regime where the entire film would consist of lamellae, as suggested by DeCaluwe et al.[69] The average distance between the channels were determined for all the films utilizing slices through the 3D reconstruction in the x-y plane (Figures S29−S39 and Zenodo[60]). The results show rather wide distributions in the values obtained for each of the films, but roughly, we can state that (i) in the 10 nm films, the distribution was centered around 12 nm, (ii) in 30 nm films around 15 nm, and (iii) in 100 nm films, around 7 nm. Thus, there was some variations in the channel distances as a function of film thickness, and the most dense channel network was observed in the 100 nm thick film, which is consistent with the highest volume fraction of the hydrophilic part (0.35 in 100 nm films vs 0.3 in 10 nm films) in that film. It is to be noted that the channel distances were determined from $x-y$ plane slices taken through the reconstructed 3D structure so that the z-direction is not the restricting dimension in the case of 10 nm thick films. Earlier

https://dx.doi.org/10.1021/acsapm.0c01318
ACS Appl. Polym. Mater. 2021, 3, 1078−1086

EFM results obtained by Barnes et al.[30] provided some insights into disconnected channels in the 100−300 nm Nafion films, and our results hopefully complete this picture by providing the 3D reconstructions of 10−100 nm films.

Our structural information about the Nafion thin films is summarized in Table 1 along with similar data collected from the literature.

As can be seen from the table, there is a rather wide distribution of channel widths reported in the literature. Data from the present study show a wider distribution in width compared to those of other reports when considering Nafion films with similar thicknesses. However, as discussed above, based on the analyses of the large number of sections through the tomograms, as presented in the Supplementary Information, it is not feasible to provide a narrower distribution. Certainly, the edges of the channels in the tomograms are diffuse and thus the measurement errors arising from that are also included in the estimation presented, and the lower and upper limits should not be taken as precise values. Furthermore, based on the collected data, there seems to be a rather small difference between channel widths in the micro- and nanometer-scale films. In fact, based on the data from, ref,[8] the range of channel widths in hundreds of micrometer thick films is quite close to ours, despite the very large difference in film thickness. Quantitative determination of phase fractions in the literature is rare. There are some qualitative estimations based on TEM imaging, but as discussed above, they tend to suffer from problems inherent for 2D imaging and cannot be considered very reliable. Results from the report by Allen et al.[36] report a value of circa 55% of hydrophilic phase, which is much higher than our values. However, as the *x-y* sectioning technique was not used in ref,[36] we argue that this inherently biases the volume fraction estimation toward 0.5. This may at least partly explain the difference. Mean distances between the channels are also rarely reported, and we could find only indirect estimates[18,68] that were rather close (8−16 nm) to the values obtained for our range of film thickness. Mean distances between the channels were also reported to be practically unaffected by the hydropilicity/phobicity of the substrate.[68]

Although the present results show perhaps even surprisingly consistent overall morphologies between all the film thicknesses on the present substrate and only marginal orientation effect for the hydrophilic channels with the thinnest films, it must be noted that the substrate itself on which the Nafion layer will be coated will strongly affect the structure of the resulting film. For example, when decreasing the film thickness, the structure is commonly expected to become more and more affected by the in-plane confinement effects coupled with surface interactions at the substrate and vapor interfaces, as described for example by Modestino et al.[57] In addition, heterogeneous substrate wetting properties can influence the preferential orientation of the hydrophobic fluorinated backbone and hydrophilic ionomer domains. The confinement effects consistent with the results reported by Modestino[57] were observed to take place also in this study with the 10 and 30 nm thick films to some degree, as discussed above. However, they were not so drastic as could have been expected based on the previous investigations.[57] Furthermore, it has been reported that the in-plane confinement and induced anisotropy of thin films can also reduce overall water uptake, that is, swelling when compared to bulk structures.[70] Based on the in situ XRR results (Table S1), there were weak indications that the overall swelling of the film was slightly less pronounced in the thinner coatings, but the results are not entirely conclusive. However, we did not see any limitations in the film's ability to self-assemble (phase separate), as suggested by Modestino[24] for very thin Nafion films, even with the thinnest 10 nm coatings. As the statements related to the loss of phase separation in thin Nafion films are based on indirect observations, they may rise from the problems related to superimposed data from the whole film, as already discussed above. Finally, the substrate topography and roughness are also likely to affect the morphology of the Nafion films. These effects are, however, outside of the scope of this study and are subject to further investigations. While Nafion literature is rich with various models[6−8,10,11,21−23,31,36,57−61,71] of films, membranes, and solutions, we can state that none of them appear to be fully consistent with our direct observations. Perhaps the closest match to our results can be found from almost identical schematics presented in refs[14,46,52] and the cluster network model discussed in a recent review by Kusoglu and Weber.[61] However, it is quite unrealistic to expect that a single structural model could represent such a complicated material as Nafion. Thus, the results from the present study show quite clearly that despite the extensive investigations carried out, there is still a lot of work to be done in characterizing thin Nafion film/substrate systems.

CONCLUSIONS

In this paper, we show directly and in fine detail the morphology of thin unannealed nanometer-scale Nafion films by STEM tomography supported by GISAXS and TEM at low temperature. Compared to existing models derived from, for example, X-ray scattering data, the real channel reconstructions reported here provide a spatial 3D illustration of the shape, size, orientation, and interconnectedness of the fine details of the channel structure in ultrathin Nafion films that have not been reported before at such a level. In particular, we show (i) how the Nafion bulk structure remains rather consistent in all three different thin-film thicknesses (10, 30, and 100 nm), from ultrathin up to thickness, which can be considered "bulk-like." (ii) The phase fractions of the hydrophobic and hydrophilic parts of the polymer are determined to be about 0.7/0.3 for the 10 nm film and changing to 0.65/0.35 for the 100 nm films. (iii) The most significant difference between the thinnest (10 nm) and thickest (100 nm) films is that in the latter films, the hydrophilic channels exhibit higher interconnectivity and some of the channels appear to end within the Nafion film instead of going through the film. (iv) Substrate-induced confinement effects start to emerge with the 10 and 30 nm thick films exhibited by the horizontal channels next to the hydrophilic SiO_2 surface. (v) Our new sample preparation method preserves characteristics of the hydrated morphology of Nafion in the dry state. (vi) A stable room temperature STEM tomography series from Nafion can be collected without observable irradiation damage using high incremental tilt angles and carbon coating. (vii) Cationic UF stain and cationic fiducial Au markers both seek the anionic hydrophilic Nafion channels. These results and sample preparation method exhibit information about the fine structure of Nafion at a level not seen before and provide a basis for a better understanding of the factors affecting the performance of very thin Nafion films in filtering applications by directly showing the branching of proton conduction channel networks in high detail.

https://dx.doi.org/10.1021/acsapm.0c01318
ACS Appl. Polym. Mater. 2021, 3, 1078−1086

MATERIAL AND METHODS

GISAXS. Silicon chips of 2 cm × 2 cm in size were dipped in a buffered hydrofluoric acid[72] for 1 min and rinsed in deionized water in order to increase Nafion adhesion for wetting experiments. On top of the silicon (100) substrate, 1 and 5% Nafion 117 was spin-coated in different thicknesses for XRR and GISAXS measurements. GISAXS measurements were performed in parallel beam mode using a Rigaku SmartLab diffractometer equipped with a 9 kW rotating Cu anode (K_{alpha} 0.154 nm), 200 um collimator, and HyPix-3000 2D detector (100 um pixel size) at a 150 mm distance. Images collected at an incidence angle of 0.5° omega were processed using Rigaku 2D Data Processing software 2DP. Measurements were carried out at room temperature and under normal humidity conditions. Nafion samples were hydrated in situ during scattering measurements by placing distilled water droplets around the beam footprint area. The beam footprint and specular directions remained free of water droplets. Consequent Nafion film wetting, that is, swelling was observed as a thickness increase during XRR measurements (Table S1 in the Supporting Information). No measurable scattering was observed for dry Nafion films. XRR scans were obtained using a K_{alpha1} monochromator, 0.05 mm vertical and 2 mm horizontal slits, and soller slits.

TEM Imaging at Low Temperature. Two types of approaches were used to image the samples at low temperatures as explained next:

Method A: Nafion 117 (Sigma-Aldrich) 5% mixture in lower aliphatic alcohols and water was spin-coated on silicon chips. Spun membranes were cut into a chessboard pattern of 9 mm^2 area squares, which were floated on deionized water and were picked up on an Agar Scientific EM grid (holey carbon 300 Cu mesh).

Method B: For cross-section imaging, 5% Nafion 117 was spin-coated as a 150 nm thick film on a solid epon (EpoFix) button, and then fresh epon was cast on top of the Nafion film to form a sandwich structure where Nafion is between epon. Then, this sandwiched button was cut into small pieces and sectioned using ultramicrotome Leica UC7 at room temperature to form cross sections of the sandwiched epon-Nafion-epon structure. Ribbons of sections that floated on the surface of water were about 50 nm in thickness. They were subsequently picked up on Agar Scientific EM grids (lacey carbon 300 Cu mesh) for TEM studies.

Both types of samples were imaged using JEOL JEM-3200FSC TEM with an Omega-type energy filter. The microscope was operated at 300 kV, and imaging was carried out under zero-loss conditions. Images were acquired with a CCD detector (Gatan Ultrascan 4000). The specimen temperature was maintained at −187 °C during imaging by liquid nitrogen cooling.

STEM Tomography. We used 5% Nafion 117 obtained from Sigma-Aldrich in a mixture of lower aliphatic alcohols and water. Thin Nafion films were fabricated by spin coating on a smooth silicon surface, with a chip size of 1.5 cm.

The stock solution 5% Nafion was used for a 100 nm film, and dilutions of 2.5 and 1% were used to achieve 30 and 10 nm thick films, respectively. After spinning, the membranes were immediately dry and were cut into a chessboard pattern of 9 mm^2 area squares. Cut films were floated on deionized water in a petri dish, and floating membrane fragments were collected on Multi A 100 × 400 mesh Au holey carbon EM grids from Quantifoil.[73] Grids, with Nafion films laid on the holey carbon side, were negatively stained with UF by blotting for 1 min. Cationic fiducial Au markers (5 and 10 nm) were added after UF blotting. UF is diluted in water until it becomes pale yellow in color, which indicates some 2.5−0.25 wt. %. Used Au nanoparticles have an additional ∼1 nm cationic ligand[74] coating on the surface approaching complete coverage. Based on their structure, the formal surface charge of the particles can be expected to be close to +1. These cationic Au particles are also highly hydrophilic with a tight hydration sheet attached to them. Last step before STEM tomography was to sputter-coat a 3 nm carbon layer for stabilizing the sample. Freestanding Nafion membranes were imaged through the holes in Multi A holey carbon using a JEOL JEM-2800 electron microscope in STEM and autofocus modes. Both bright field and dark field 16 bit mrc stacks were collected using a TEMography Recorder program for the STEM tilt series. Nominal magnification of 800 k and 1 M was used, giving pixel sizes of 0.337 and 0.27 nm, respectively. A quickie STEM method (P. Engelhardt, unpublished data), that is, tilt series collected with spanning −72 to +72, with 8 degree increment steps under low dose mode, 200 kV, camera length 4 m, 155 μA emission current, 1.5 e^{-5} Pa microscope chamber vacuum, and probe size 0.2 nm was used. In addition to less time spent on series, using tilt series of 8° increments reduces the exposure dose down to 26% of conventional series taken at 2° increments, making stable Nafion imaging possible at RT.

EMAN2 (e2projectManager) was used to convert 16 bit to 32 bit mrc stack. For alignment of the stacks, ETOMO[75] automatic (coarse fiducialles) alignment mode was used. The maximum entropy method was used for 3D reconstruction[76,77] and UCSF Chimera was used for visualization of 3D reconstructions.

ASSOCIATED CONTENT

Supporting Information

The Supporting Information is available free of charge at https://pubs.acs.org/doi/10.1021/acsapm.0c01318.

Movies of 3D reconstructions of Nafion thin films, that are available free of charge via the internet at Zenodo (DOI: 10.5281/zenodo.3784525) and supplementary material images at Zenodo (DOI: 10.5281/zenodo.4276343). (PDF)

AUTHOR INFORMATION

Corresponding Author

A. Peltonen − *Aalto-NanoFab, Micronova, Aalto University, Espoo 02150, Finland*; Email: antti.peltonen@aalto.fi

Authors

J. Etula − *Department of Chemistry and Materials Science, School of Chemical Engineering, Aalto University, Espoo 02150, Finland*; orcid.org/0000-0002-6930-1165

J. Seitsonen − *Nanomicroscopy Center (NMC), Department of Applied Physics, Aalto University, Espoo 02150, Finland*

P. Engelhardt − *Nanomicroscopy Center (NMC), Department of Applied Physics, Aalto University, Espoo 02150, Finland*

T. Laurila − *Department of Chemistry and Materials Science, School of Chemical Engineering, Aalto University, Espoo 02150, Finland; Department of Electrical Engineering and Automation, School of Electrical Engineering, Aalto University, Espoo 02150, Finland*

Complete contact information is available at: https://pubs.acs.org/10.1021/acsapm.0c01318

Notes

The authors declare no competing financial interest.

ACKNOWLEDGMENTS

The authors appreciate the support of the Otanano Otaniemi Research Infrastructure for Micro and Nano Technologies. Samples were fabricated in the Micronova Nanofabrication Centre of Aalto University, and imaging was done at Nanomicroscopy Center of Aalto University. T.L. acknowledges support from European Union's Horizon 2020 Research and Innovation Programme H2020-FETPROACT-2018-01 under grant agreement No. 824070.

REFERENCES

(1) Leppänen, E.; Peltonen, A.; Seitsonen, J.; Koskinen, J.; Laurila, T. Effect of thickness and additional elements on the filtering

properties of a thin Nafion layer. *J. Electroanal. Chem.* **2019**, *843*, 12−21.
(2) Choi, P.; Jalani, N. H.; Datta, R. Thermodynamics and proton transport in Nafion II. proton diffusion mechanisms and conductivity. *J. Electrochem. Soc.* **2005**, *152*, E123−E130.
(3) Thampan, T.; Malhotra, S.; Tang, H.; Datta, R. Modeling of conductive transport in proton-exchange membranes for fuel cells. *J. Electrochem. Soc.* **2000**, *147*, 3242.
(4) Zawodzinski, T. A.; Davey, J.; Valerio, J.; Gottesfeld, S. The Water content dependence of electro-osmotic drag in proton-conducting polymer electrolytes. *Electrochim. Acta* **1995**, *40*, 297−302.
(5) Doyle, M.; Wang, L.; Yang, Z.; Choi, S. K. Polymer electrolytes based on ionomer copolymers of ethylene with fluorosulfonate functionalized monomers. *J. Electrochem. Soc.* **2003**, *150*, D185.
(6) Elliott, J. A.; Hanna, S.; Elliott, A. M. S.; Cooley, G. E. Interpretation of the small-angle x-ray scattering from swollen and orientated perfluorinated ionomer membranes. *Macromolecules* **2000**, *33*, 4161−4171.
(7) Gebel, G.; Diat, O. Neutron and x-ray scattering: Suitable tools for studying ionomer membranes. *Fuel Cells* **2005**, *5*, 261−276.
(8) Rubatat, L.; Gebel, G.; Diat, O. Fibrillar structure of Nafion: matching Fourier and real space studies of corresponding films and solutions. *Macromolecules* **2004**, *37*, 7772−7783.
(9) Gebel, G.; Lambard, J. Small-angle scattering study of water-swollen perfluorinated ionomer membranes. *Macromolecules* **1997**, *30*, 7914−7920.
(10) Haubold, H. G.; Vad, T.; Jungbluth, H.; Hiller, P. Nanostructure of Nafion: A SAXS study. *Electrochim. Acta* **2001**, *46*, 1559−1563.
(11) van der Heijden, P. C.; Rubatat, L.; Diat, O. Orientation of drawn Nafion at molecular and mesoscopic scales. *Macromolecules* **2004**, *37*, 5327−5336.
(12) Kreuer, D.-K.; Portale, G. A Critical revision of the nano-morphology of proton conducting ionomers and polyelectrolytes for fuel cell applications. *Adv. Funct. Mater.* **2013**, *23*, 5390−5397.
(13) Wisniewski, N.; Reichert, M. Methods for reducing biosensor membrane biofouling. *Colloids Surf., B* **2000**, *18*, 197−219.
(14) Mauritz, K. A.; Moore, R. B. State of understanding Nafion. *Chem. Rev.* **2004**, *104*, 4535−4586.
(15) Gierke, T. D.; Munn, G. E.; Wilson, F. C. The Morphology in Nafion perfluorinated membrane products, as determined by wide- and small-angle x-ray studies. *J. Polym. Sci., Polym. Phys. Ed.* **1981**, *19*, 1687−1704.
(16) Chang, X. L., Chee, P. S., Lim, E. H. A Microreservoir-based drug delivery device using ionic polymer metal composite (IPMC) actuator. *TENCON, 2018 − 2018 IEEE Region 10 Conference*, 2018.
(17) Rollet, A. L.; Diat, O.; Gebel, G. A New insight into Nafion structure. *J. Phys. Chem. B* **2002**, *106*, 3033−3036.
(18) Rubatat, L.; Rollet, A. L.; Gebel, G.; Diat, O. Evidence of elongated polymeric aggregates in Nafion. *Macromolecules* **2002**, *35*, 4050−4055.
(19) Fujimura, M.; Hashimoto, T.; Kawai, H. Small-angle x-ray scattering study of perfluorinated ionomer membranes. 1. Origin of two scattering maxima. *Macromolecules* **1981**, *14*, 1309−1315.
(20) Gebel, G.; Moore, R. B. Small-angle scattering study of short pendant chain perfluoro sulfonated ionomer membranes. *Macromolecules* **2000**, *33*, 4850−4855.
(21) Gebel, G. Structural evolution of water swollen perfluorosulfonated ionomers from dry membrane to solution. *Polymer* **2000**, *41*, 5829−5838.
(22) Fujimura, M.; Hashimoto, T.; Kawai, H. Small-angle x-ray scattering study of perfluorinated ionomer membranes. *Macromolecules* **1981**, *14*, 1309−1315.
(23) Bass, M.; Berman, M.; Singh, A.; Konovalov, O.; Freger, V. Surface structure of Nafion in vapor and liquid. *J. Phys. Chem. B* **2010**, *114*, 3784−3790.
(24) Modestino, M. A.; Paul, D. K.; Dishari, S.; Petrina, S. A.; Allen, F. I.; Hickner, M. A.; Karan, K.; Segalman, R. A.; Weber, A. Z. Self-assembly and transport limitations in confined Nafion films. *Macromolecules* **2013**, *46*, 867−873.
(25) Kwon, O.; Liu, Y.; Zhu, E.; Wu, S.; Zhu, D. Current sensing atomic force microscopy study of thermal aging of Nafion membranes. *J. Phys. Chem. C* **2017**, *121*, 7741−7749.
(26) Doyle, M.; Rajendran, G. Perfluorinated membranes. *Handbook of Fuel Cells*, 2010, DOI: 10.1002/9780470974001.f303034.
(27) He, Q.; Kusoglu, A.; Lucas, I. T.; Clark, K.; Weber, A. Z.; Kostecki, R. Correlating humidity-dependent ionically conductive surface area with transport phenomena in proton-exchange membranes. *J. Phys. Chem. B* **2011**, *115*, 11650−11657.
(28) Bussian, D. A.; O'Dea, J. R.; Metiu, H.; Buratto, S. K. Nanoscale current imaging of the conducting channel in proton exchange membrane fuel cells. *Nano Lett.* **2007**, *7*, 227−232.
(29) Aleksandrova, E.; Hiesgen, R.; Friedrich, K. A.; Roduner, E. Electrochemical atomic force microscopy study of proton conductivity in a Nafion membrane. *Phys. Chem. Chem. Phys.* **2007**, *9*, 2735−2743.
(30) Barnes, A. M.; Buratto, S. K. Imaging channel connectivity in Nafion using electrostatic force microscopy. *J. Phys. Chem. B* **2018**, *122*, 1289−1295.
(31) Rieberer, S.; Norian, K. H. Analytical electron microscopy of Nafion ion exchange membranes. *Ultramicroscopy* **1992**, *41*, 225−233.
(32) Ceynowa, J. Electron microscopy investigation of ion exchange membranes. *Polymer* **1978**, *19*, 73−76.
(33) Porat, Z.; Fryer, J. R.; Huxman, M.; Rubinstein, I. Electron microscopy investigation of the microstructure of Nafion films. *J. Phys. Chem.* **1995**, *99*, 4667−4671.
(34) Fujimura, M.; Hashimoto, T.; Kawai, H. Small-angle x-ray scattering study of perfluorinated ionomer membranes. 2. Models for ionic scattering maximum. *Macromolecules* **1982**, *15*, 136−144.
(35) Xue, T.; Trent, J. S.; Osseo-Asare, K. J. Characterization of Nafion membranes by transmission electron microscopy. *J. Membr. Sci.* **1989**, *45*, 261−271.
(36) Allen, F. I.; Comolli, L. R.; Kusoglu, A.; Modestino, M. A.; Minor, A. M.; Weber, A. Z. Morphology of hydrated as-cast Nafion revealed through cryo electron tomography. *ACS Macro Lett.* **2015**, *4*, 1−5.
(37) Yakovlev, S.; Balsara, N.; Downing, K. Insights on the study of Nafion nanoscale morphology by transmission electron microscopy. *Membranes* **2013**, *3*, 424−439.
(38) Dreyfus, B.; Gebel, G.; Aldebert, P.; Pineri, M.; Escoubes, M.; Thomas, M. Distribution of the 'micelles' in hydrated perfluorinated ionomer membranes from SANS experiments. *J. Phys.* **1990**, *51*, 1341−1354.
(39) Rollet, A. L.; Gebel, G.; Simonin, J. P.; Turq, P. A SANS determination of the influence of external conditions on the nanostructure of Nafion membrane. *J. Polym. Sci. B Polym. Phys.* **2001**, *39*, 548.
(40) Roche, E. J.; Pineri, M.; Duplessix, R. Phase separation in perfluorosulfonate ionomer membranes. *J. Polym. Sci., Polym. Phys. Ed.* **1982**, *20*, 107−116.
(41) Kim, M. H.; Glinka, C. J.; Grot, S. A.; Grot, W. G. SANS study of the effects of water vapor sorption on the nanoscale structure of perfluorinated sulfonic acid (Nafion) membranes. *Macromolecules* **2006**, *39*, 4775−4787.
(42) Dura, J. A.; Murthi, V. S.; Hartman, M.; Satija, S. K.; Majkrzak, C. F. Multilamellar interface structures in Nafion. *Macromolecules* **2009**, *42*, 4769−4774.
(43) Falk, M. An infrared study of water in perfluorosulfonate Nafion membranes. *Can. J. Chem.* **1980**, *58*, 1495−1501.
(44) Heitner-Wirguin, C. Infra-red spectra of perfluorinated cation-exchanged membranes. *Polymer* **1979**, *20*, 371.
(45) Yeager, H. L.; Steck, A. Cation and water diffusion in Nafion ion exchange membranes: influence of polymer structure. *J. Electrochem. Soc.* **1981**, *128*, 1880−1884.
(46) Kreuer, K. D. On the development of proton conducting polymer membranes for hydrogen and methanol fuel cells. *J. Membr. Sci.* **2001**, *185*, 29−39.

(47) Hickner, M. A.; Ghassemi, H.; Kim, Y. S.; Einsla, B. R.; McGrath, J. E. Alternative polymer systems for proton exchange membranes (PEMs). *Chem. Rev.* **2004**, *104*, 4587−4612.
(48) Litt, M. H. A Reevaluation of Nafion morphology. *Polym. Prepr.* **1997**, *38*, 80.
(49) Hsu, W. Y.; Gierke, T. D. Elastic theory for ionic clustering in perfluorinated ionomers. *Macromolecules* **1982**, *15*, 101−105.
(50) Schmidt-Rohr, K.; Chen, Q. Parallel cylindrical water nanochannels in Nafion fuel-cell membranes. *Nat. Mater.* **2008**, *7*, 75−83.
(51) Marx, C. L.; Caulfield, D. F.; Cooper, S. L. Morphology of ionomers. *Macromolecules* **1973**, *6*, 344−353.
(52) Kreuer, K. D.; Paddison, S. J.; Spohr, E.; Schuster, M. Transport in proton conductors for fuel-cell applications: simulations, elementary reactions, and phenomenology. *Chem. Rev.* **2004**, *104*, 4637−4678.
(53) Cwirko, E. H.; Carbonell, R. G. Interpretation of transport coefficients in Nafion using a parallel pore model. *J. Membr. Sci.* **1992**, *67*, 227−247.
(54) Choi, P.; Jalani, N. H.; Datta, R. Thermodynamics and proton transport in Nafion III. proton transport in Nafion/sulfated ZrO_2 nanocomposite membranes. *J. Electrochem. Soc.* **2005**, *152*, A1548−A1554.
(55) Hsu, W. Y.; Gierke, T. D. Ion transport and clustering in Nafion perfluorinated membranes. *J. Membr. Sci.* **1983**, 307−326.
(56) Danbolt, N. C. Glutamate uptake. *Prog. Neurobiol.* **2001**, *65*, 1−105.
(57) Modestino, M. A.; Kusoglu, A.; Hexemer, A.; Weber, A. Z.; Segalman, R. A. Controlling Nafion Structure and Properties Via Wetting Interactions. *Macromolecules* **2012**, *45*, 4681−4688.
(58) Elliott, J. A.; Wu, D.; Paddison, S. J.; Moore, R. B. A Unified Morphological Description of Nafion Membranes From SAXS and Mesoscale Simulations. *Soft Matter* **2011**, *7*, 6820−6827.
(59) Lucks, C.; Rossberg, A.; Tsushima, S.; Foerstendorf, H.; Fahmy, K.; Bernhard, G. Formic acid interaction with the uranyl(VI) ion: structural and photochemical characterization. *Dalton Trans.* **2013**, *42*, 13584.
(60) Peltonen, A. Three-Dimensional Fine Structure of Nanometer Scale Nafion Thin Films, DOI: 10.5281/zenodo.4276343.
(61) Kusoglu, A.; Weber, A. Z. New insights into perfluorinated sulfonic-acid ionomers. *Chem. Rev.* **2017**, *117*, 987−1104.
(62) Duplessix, R.; Escoubes, M.; Rodmacq, B.; Volino, F.; Roche, E.; Eisenberg, A.; Pineri, M. Water absorption in acid Nafion membranes, water in polymers. *ACS* **1980**, *28*, 469−486.
(63) Peltonen, A. Nafion STEM tomography 3D reconstructions (Version 1.0). *Zenodo.* , DOI: 10.5281/zenodo.3784525.
(64) Kushner, D. I.; Kusoglu, A.; Podraza, N. J.; Hickner, M. A. Substrate-dependent molecular and nanostructural orientation of Nafion thin films. *Adv. Funct. Mater.* **2019**, *29*, No. 1902699.
(65) Vanya, P.; Sharman, J.; Elliott, J. A. Mesoscale simulations of confined Nafion thin films. *J. Chem. Phys.* **2017**, *147*, 214904.
(66) Sengupta, S.; Lyulin, A. V. Molecular dynamics simulations of substrate hydrophilicity and confinement effects in capped nafion films. *J. Phys. Chem. B* **2018**, *122*, 6107−6119.
(67) Eastman, S. A.; Kim, S.; Page, K. A.; Rowe, B. W.; Kang, S.; Soles, C. L.; Yager, K. G. Effect of confinement on structure, water solubility, and water transport in Nafion thin films. *Macromolecules* **2012**, *45*, 7920−7930.
(68) Kim, S.; Dura, J. A.; Page, K. A.; Rowe, B. W.; Yager, K. G.; Lee, H. J.; Soles, C. L. Surface-induced nanostructure and water transport of thin proton-conducting polymer films. *Macromolecules* **2013**, *46*, 5630−5637.
(69) DeCaluwe, S. C.; Baker, A. M.; Bhargava, P.; Fischer, J. E.; Dura, J. A. Structure-property relationships at Nafion thin-film interfaces: Thickness effects on hydration and anisotropic ion transport. *Nano Energy* **2018**, *46*, 91−100. 1902699, 2019
(70) Kusoglu, A.; Kienitz, B. L.; Weber, A. Z. Understanding the effects of compression and constraints on water uptake of fuel-cell membranes. *J. Electrochem. Soc.* **2011**, *158*, B1504. Available from
(71) Kusoglu, A.; Dursch, T. J.; Weber, A. Z. Nanostructure/Swelling relationships of bulk and thin-film PFSA ionomers. *Adv. Funct. Mater.* **2016**, *26*, 4961−4975.
(72) Honeywell, 10579892, AF 90-10 LST VLSI Puranal, Ammonium fluoride etching mixture.
(73) Quantifoil, www.quantifoil.com/
(74) Hassinen, J.; Liljeström, V.; Kostiainen, M. A.; Ras, R. H. A. Rapid cationization of gold nanoparticles by two-step phase transfer. *Angew. Chem., Int. Ed.* **2015**, *54*, 7990−7993.
(75) Kremer, J. R.; Mastronarde, D. N.; McIntosh, J. R. Computer visualization of three-dimensional image data using IMOD. *J. Struct. Biol.* **1996**, *116*, 71−76.
(76) Engelhardt, P. Three-dimensional reconstruction of chromosomes using electron tomography. *Methods Mol. Biol.* **2007**, *369*, 365−385.
(77) Engelhardt, P. *Electron tomography of chromosome structure. Encycl. Anal. Chem.* , John Wiley & Sons Ltd., 2006.

https://dx.doi.org/10.1021/acsapm.0c01318
ACS Appl. Polym. Mater. 2021, 3, 1078−1086